11 WCEE
Published by Elsevier Science Ltd 1996
Paper No. 768. (quote when citing this article)
Eleventh World Conference on Earthquake Engineering
ISBN: 0 08 042822 3

DIAPHRAGM ACTION OF PRECAST FLOORS: BEHAVIOR AND MODELING

M. MENEGOTTO and G. MONTI

Dipartimento di Ingegneria Strutturale e Geotecnica, Università La Sapienza
Via A. Gramsci 53, 00197 Roma, Italy

ABSTRACT

The analytical model is elaborated of a "continuous waved shear key" joint, shaped as a sinusoidal profile, located at the interface between adjacent precast floor slabs. The aim of the joint is to provide floors with adequate in-plane strength and stiffness, making them able to distribute the seismic forces among vertical resisting elements. The performance of this joint is extremely effective under cyclic action of high intensity, as assessed in a series of experimental tests. In this paper, an interface finite element is developed, in which the joint response is condensed into two degrees of freedom, *i.e.* the relative displacements, parallel and orthogonal to the joint, between two nodes of adjacent precast units. The relationship between these two d.o.f.'s is ruled by a constraint equation based on the wave profile. When a relative displacement is imposed parallel to the interface, it develops a resisting mechanism, contributed by the *wedge effect* of the undulated profiles and by the friction rising at their contact. The model reproduces correctly this behavior, able to resist in-plane actions even in the absence of friction, provided transverse confinement is present. The stiffness matrix is set up also considering the possibility of having the joint open, which may happen when dealing with complete decks acted on by in-plane shear and bending. The analytical modeling of this connecting element allows for numerical tests on different floor configurations.

KEYWORDS

Seismic analysis, Building Structures, Precast Floors, Diaphragm Action, Shear Joints, Waved Profiles.

INTRODUCTION

In buildings, floors primarily sustain the vertical loads, but have also the role of linking columns and walls at each level to a common horizontal displacement. The "diaphragm action" allows for a distribution among vertical elements of the wind- or earthquake-induced horizontal forces. Normally, monolithic concrete slabs may easily fulfill stiffness and strength requirements, provided they are well detailed. Therefore their in-plane behavior is usually paid little attention, under the assumption, usually made in the seismic design of buildings, that the idealized behavior is automatically observed. On the other hand, in the design of precast structures this behavior cannot be assured *a priori*, since it depends on the adopted shear transfer mechanism between precast units. For example, prefabricated hollow-core slabs realize long span floors (more than 20 m). These slabs are extruded on mouldless long-line beds, their only reinforcement being longitudinal prestressed strands. The joints between parallel slabs are grouted *in situ* with mortar and the beam-to-slab joints are grouted with connecting tie-reinforcement. Possibly, no structural concrete is cast on top of the slabs, since it implies

additional self-weight and consequent increase of seismic forces. It is clear that the effectiveness of the diaphragm action relies on the joints. For this reason, a new type of joint has been developed. A comprehensive report on its development and testing, as well as general references, can be found in (Menegotto 1994).

THE UNDULATED JOINT

The joint has a waved profile of small amplitude (2.5 mm), represented in Fig. 1. This is a special longitudinal joint between adjacent precast units, profiled with a continuous undulated shear key, and purposedly realized for improving the resistance to in-plane shear forces. The particular profile, associated with a transverse restraint, implies in principle the increase of friction force with increasing displacement, beyond the most severe structural local deformation. The transverse restraint in real decks is exerted by tie-beams surrounding them. The joint does not degradate sensibly after severe load reversals. It leads to energy dissipation for friction during the shear dsplacements, which is favorable under dynamic action, even if normally it will not be accounted for, being demanded to other structural parts.

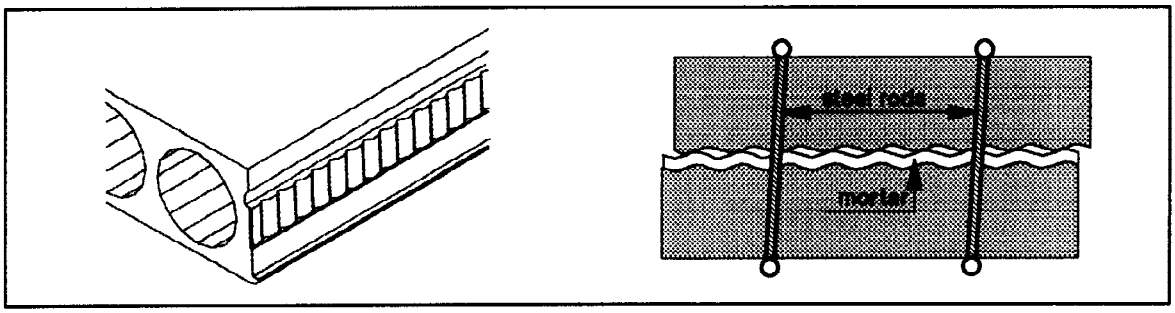

Fig. 1. View of the undulated joint (left) and scheme of short samples tested (right).

EXPERIMENTAL CAMPAIGN

The experimental research has developed along eight years, with tests on both short laboratory specimens of the waved joint (Menegotto and Morelli 1984) and large full-scale untopped decks, incorporating the waved joints (Menegotto 1988; Menegotto and Monti 1988). The study aimed both at evaluating the strength and stiffness characteristics of the joint and at improving and testing the behavior of extruded hollow-core slabs without *in situ* topping in their diaphragm action under seismic conditions. A first part of the experimental research has been performed on samples of joints, 1.0 m long, for different slab depths. The testing scheme is shown in Fig. 1. The sample is fixed horizontally on a suspended twin steel frame, by means of which an alternate reversing shear force is applied to the joint, precisely along its axis. Four external hinged steel rods hold the sample halves tight together, simulating the effect of tie-beams exerting a compressive transverse force on the joint and governing the friction. Most joints were artificially pre-cracked, by means of a vertical bending load, in order to simulate possible unfavorable service conditions. About 30 samples were tested and a typical result of one test is shown in Fig. 7, in terms of force-displacement diagram. Some conclusions were derived, which may be summarized as follows. The shear response of the pre-cracked joint is depending on the transverse restraint; hence, the importance of sufficiently stiff tying of the structure is emphasized. For small relative displacements (<2 mm), also cyclic, an average shear resistance of 0.5 N/mm^2 (referred to the height of the waved profile of 95 mm) may be relied upon, with a minimum tying at the deck's edges. For greater displacements, the resisting shear force grows. This strain-hardening behavior represents a very sound feature. After cycles of severe loading reversals, the shear resistance does not lower sensibly which is also a major aspect of sound behavior, contrary to what has been shown by plain or indented joints.

While the tests on short joints specimens had the scope of adjusting and checking the surface shape and its local behavior, tests on full decks check the behavior in more realistic conditions, accounting for joints length, combined bending, real stiffness of tie-beams and surrounding structure (Fig. 2). Decks spanned up to 12 m, and were of 6 m wide (five precast hollow-core units). The tested model represents structural conditions where the deck is a horizontal cantilever, fixed along a side joint of a slab. Thus, that joint is subjected to both in-plane maximum shear and bending, when horizontal forces, applied by means of two jacks, act on the deck. A concrete platform provides bulkheads for counteracting the jacks and for clamping fixed slabs and tie-beams.

These tests on complete decks confirmed the resistance capacity of joints and gave further information. Joints show high stiffness under service conditions, such that the decks may be considered as rigid. The horizontal forces reached in the different tests were such that the corresponding shear stresses were 0.42-0.95 N/mm^2. The ability of the surrounding tie-beams, even weak ones, to exert a restraint on long joints, though placed only at their ends, was proved. In all tests, the tie beam reinforcement came to yield, showing that the mechanism is able to mobilize its entire capacity. However, the applied forces were always larger than possible design forces. The test results were of similar appearance as those of the tests on one joint specimen in Fig. 7, but the curves are less regular with respect to the isolated joints, due to interactions of all parts of the whole structure, cracks, adaptations of connections, yielding of tie-beam, and so on.

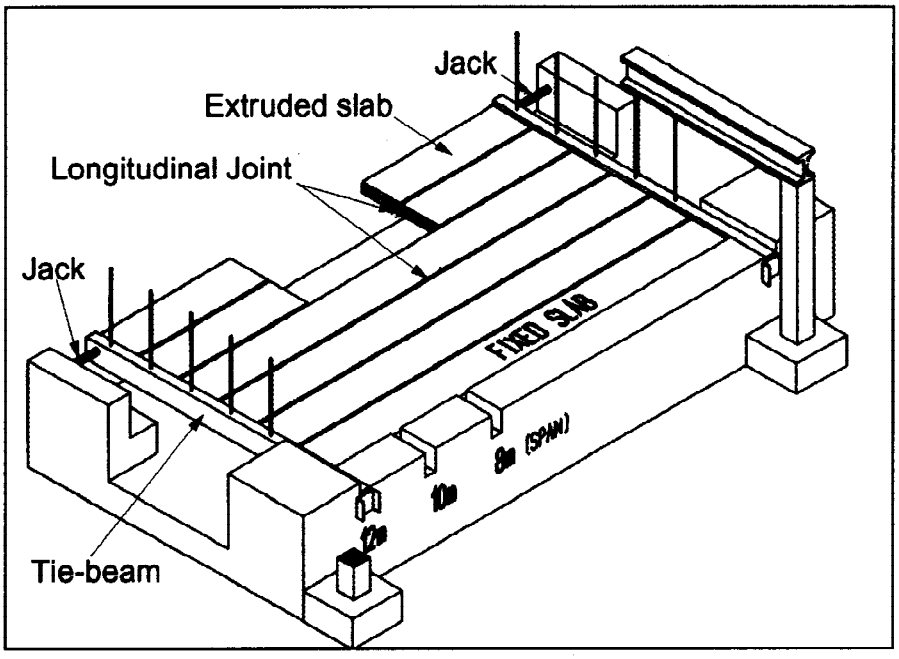

Fig. 2. Full scale decks testing setup.

GOVERNING EQUATIONS OF THE JOINT

Sliding of simusoidal profiles

Two sinusoidal profiles of amplitude A and wavelength λ are considered (Fig. 3). The profiles are identified by the two equations:

$$y_1(x) = A \sin\frac{2\pi}{\lambda}x \tag{1}$$

$$y_2(x,s) = w(s) + A \sin\frac{2\pi}{\lambda}(x-s) \tag{2}$$

The former represents a fixed profile, while the latter is that of a moving profile which, starting from a position of perfect superposition, slides longitudinally on the former by a quantity s and moves away of a quantity w. The function $w(s)$ represents the constraint equation, which links the relative opening to the relative slide of the two profiles. The determination of $w(s)$ is based on two conditions: a) the two profiles always have a contact point; b) the contact occurs between two points with the same tangent.
These two conditions are expressed, respectively, by:

$$A \sin\frac{2\pi}{\lambda}x = w(s) + A \sin\frac{2\pi}{\lambda}(x-s) \tag{3}$$

$$\frac{2\pi}{\lambda}A \cos\frac{2\pi}{\lambda}x = \frac{2\pi}{\lambda}A \cos\frac{2\pi}{\lambda}(x-s) \tag{4}$$

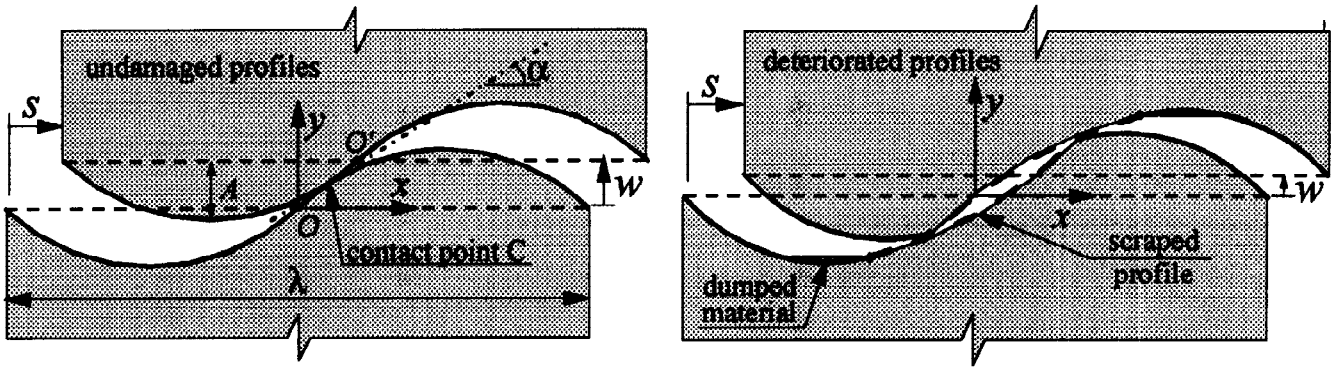

Fig. 3. Sinusoidal profiles subjected to relative sliding. Initial profiles (left) and deteriorated profiles (right).

From Eq. (4), the abscissa x_C of the contact point C is obtained:

$$x_C = \frac{s}{2} \tag{5}$$

which indicates that the contact point C between two profiles is always located at half of the relative sliding of two points initially superposed at the origin (O and O' in Fig. 3).
Substituting Eq. (5) into Eq. (3), the sought expression for w is obtained:

$$w = 2A \sin\frac{\pi}{\lambda}|s| \tag{6}$$

where the absolute value of s and the resulting positiveness of w, indicate that the two profiles transversely move away, both for positive and negative values of the relative sliding.

It should be noted that the maximum distance $2A$ between the two profiles, is obtained for a relative sliding s equal to half wavelength (Fig. 4). In this situation, the contact point is located at $x_C = \lambda/4$, on the peaks of the sinusoids. Any increase of the relative sliding will bring the two profiles closer. However, the wavelength has been chosen so to avoid this occurrence in practical conditions.

The variation of the tangent at the contact point C (Fig. 3) is given by:

$$\tan\alpha_C = 2A\frac{\pi}{\lambda}\cos\frac{\pi}{\lambda}|s| \cdot \operatorname{sgn} s \tag{7}$$

where sgn denotes the sign function. Note that the first sliding (s= 0) occurs with initial angle $\alpha_O = 2\pi A/\lambda$, equal to the slope of the tangent at the origin of the sinusoids.
Eqs. (6) and (7) are represented in Fig. 4, for profiles with A = 2.5 mm and λ = 50 mm.

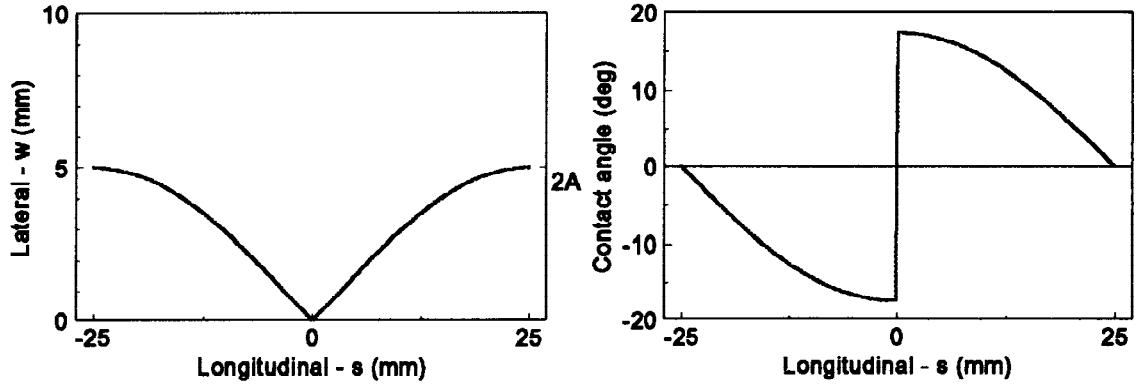

Fig. 4. Sinusoidal profiles: lateral displacement vs. sliding (left), slope at contact point vs. sliding (right).

Sliding of scraped sinusoidal profiles

In case of perfect profiles, the contact point is unique and moving along the convex portions of the sinusoids. Due to the persisting contact, the two profiles are subjected to scraping effect which modifies the shape of the profiles in a complex way, so that in reality multiple contact points can be present at the same time and vary irregularly. Since a pointwise modelization along a continuous wave of such a complicated phenomenon would be inexpedient, an average profile alteration, typical for the whole profile, has been assumed (Fig. 3). A constraint equation, based on the joint profile and made to vary depending on the damage due to scraping effect between profiles, has been developed (Menegotto and Monti 1995).

Determination of the longitudinal force

Two sinusoidal profiles, subjected to relative sliding under transverse confinement, generate in the direction of sliding a resisting force F_s, contributed by two parallel mechanisms: a *wedge-action*, depending on the instantaneous slope α of the tangent at the contact point, while the second is a friction mechanism between two profiles, depending on the friction angle φ. Sliding occurs if the following equality is satisfied (Fig. 5):

$$F_s = F_w \tan(\alpha_C + \varphi \cdot \operatorname{sgn} \dot{s}) \tag{8}$$

where sgn denotes the sign function and $\dot{s}$ is the relative sliding velocity between the two profiles.

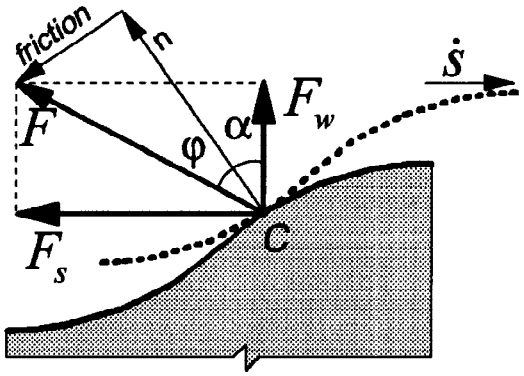

Fig. 5. Components of the forces acting at the contact point C of two sinusoidal profiles.

FINITE ELEMENT OF THE JOINT

The constraint and equilibrium equations described above are the basis for the development of a finite element which models the behavior of the undulated joint. In view of the modelization of an entire deck, whose mesh includes shell elements for the slab and beam elements for the tie beams, the finite element for the undulated joint is developed as a two-node element which connects the corner points of two adjacent shell elements discretizing the precast slab units (Fig. 6). The element has therefore four d.o.f.'s: $\mathbf{U} = \{u_1 \quad v_1 \quad u_2 \quad v_2\}$, which are transformed into the local d.o.f.'s w and s, defined in the previous section, as follows

$$\mathbf{u} = \mathbf{R} \cdot \mathbf{U} \quad \rightarrow \quad \begin{Bmatrix} w \\ s \end{Bmatrix} = \begin{bmatrix} -1 & 0 & 1 & 0 \\ 0 & -1 & 0 & 1 \end{bmatrix} \cdot \mathbf{U} \tag{9}$$

These local d.o.f.'s are linked through the constraint equation, Eq. (6), which introduces an internal constraint and obliges both nodes to move relatively to each other on the line given by the sinusoidal profile. For the time being, no damaged profile was modeled in the finite element. When dealing with complete decks, the constraint equation is modified into

$$w \geq 2A \sin\frac{\pi}{\lambda}|s| \tag{10}$$

because also opening (*i.e.*, loss of contact) of the joints are allowed.

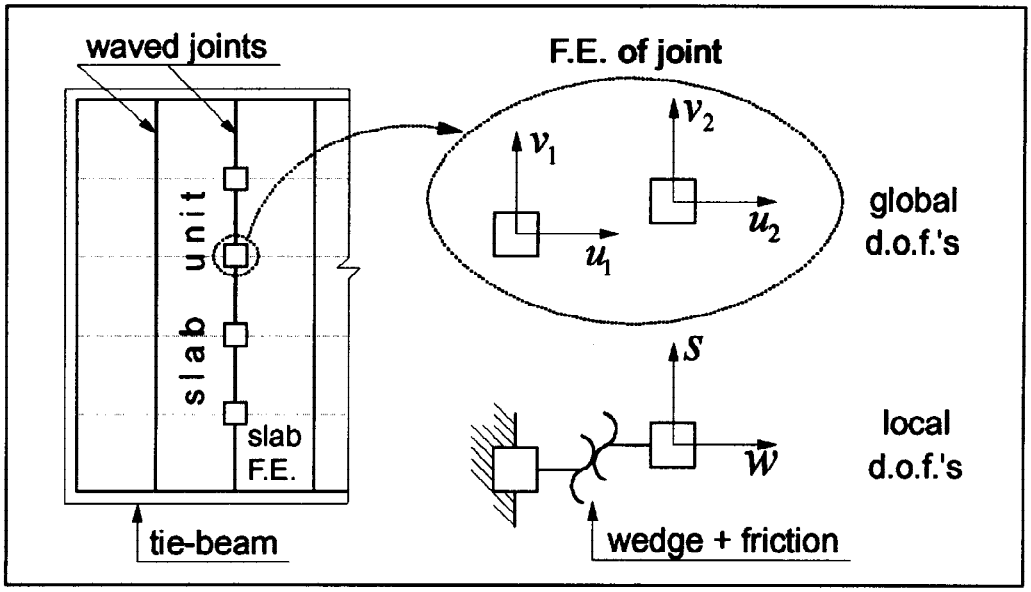

Fig. 6. Finite element of longitudinal joint between adjacent precast slab units.

In order to comply with this internal constraint, the finite element is formulated by means of the so-called 'penalty method', which allows to write a constrained variational principle, that is, a functional including the constraint equation, as follows

$$\Pi = k \cdot \left(w - 2A \cdot \sin \frac{\pi}{\lambda} |s| \right)_-^2 \tag{11}$$

where $(\ )_-$ indicates that, due to Eq. (10), only the negative part of the constraint equation is considered, and k is a 'penalty number'. The solution obtained by the stationarity of the functional Π will satisfy the constraint only approximately. The larger the value of k the better will be the constraint achieved. Performing the variation of Π with respect to w and s, one obtains

$$\begin{aligned} \frac{\partial \Pi}{\partial w} &= k \left(w - 2A \sin \frac{\pi}{\lambda} |s| \right)_- \cdot \delta w = 0 \\ \frac{\partial \Pi}{\partial s} &= -k \left(w - 2A \sin \frac{\pi}{\lambda} |s| \right)_- 2A \frac{\pi}{\lambda} \cos \frac{\pi}{\lambda} |s| \cdot \operatorname{sgn} s \cdot \delta s = 0 \end{aligned} \tag{12}$$

and, after eliminating the variation quantities δw and δs with the standard argument of arbitrarity, the two equations are obtained, which are to be satisfied at the same time

$$\begin{aligned} k \left(w - 2A \sin \frac{\pi}{\lambda} |s| \right)_- &= F_{w,res} \\ -k \left(w - 2A \sin \frac{\pi}{\lambda} |s| \right)_- 2A \frac{\pi}{\lambda} \cos \frac{\pi}{\lambda} |s| \cdot \operatorname{sgn} s &= F_{s,res} \end{aligned} \tag{13}$$

where ΔF_{res} are the residuals.

The first equation represents the restoring force that the element exerts when a displacement is applied in the direction w, while the second equation represents the restoring force for a displacement applied along s. Both forces are contact forces which prevent the two sliding profiles from compenetrating. It should be recognized that, considering Eq. (7), the second equation can be rewritten as

$$-k \left(w - 2A \sin \frac{\pi}{\lambda} |s| \right)_- \tan \alpha_C = F_{s,res} \tag{14}$$

which basically implies that the *wedge-action* depending on the instantaneous slope α of the tangent at the contact point is implicitly accounted for by satisfying the second equation.

Due to the nonlinear character of the phenomenon, the tangent stiffness matrix is obtained through linearization of Eqs. (13), using Eq. (7), as follows

$$\begin{aligned} & k\cdot\Delta w - k\tan\alpha_C\cdot\Delta s = \Delta F_{w,res} \\ & -k\tan\alpha_C\cdot\Delta w + \left(2k\tan^2\alpha_C + 2kA\frac{\pi^2}{\lambda^2}\left(w\sin\frac{\pi}{\lambda}|s| - 2A\right)\right)\cdot\Delta s = \Delta F_{s,res} \end{aligned} \tag{15}$$

Eqs. (15) can be written in matrix form, to yield the local (as expected, symmetric) stiffness matrix **K**:

$$\left[\begin{array}{c|c} k & -k\tan\alpha_C \\ \hline -k\tan\alpha_C & 2k\tan^2\alpha_C + 2kA\frac{\pi^2}{\lambda^2}\left(w\sin\frac{\pi}{\lambda}|s| - 2A\right) \end{array}\right]\cdot\Delta\mathbf{u} = \mathbf{K}\cdot\Delta\mathbf{u} = \Delta\mathbf{F}_{u,res} \tag{16}$$

where, as above, Eq. (7) was used, and $\Delta\mathbf{F}_{u,res}$ represents the residuals vector.

Friction is an additional force that modifies Eq. (14), in compliance with Eq. (8), as follows

$$-k\left(w - 2A\sin\frac{\pi}{\lambda}|s|\right)^{-}\tan(\alpha_C + \varphi\cdot\operatorname{sgn}\dot{s}) = F_{s,res} \tag{17}$$

The modifications introduced in the stiffness matrix by the friction action are obtained through linearization of the above equation, with respect to w and s, respectively

$$\begin{aligned} & \mathbf{K}_{1,2} = \mathbf{K}_{2,1} = -k\tan(\alpha_C + \varphi\cdot\operatorname{sgn}\dot{s}) \\ & \mathbf{K}_{2,2} = k\tan\alpha_C\cdot\tan(\alpha_C + \varphi\cdot\operatorname{sgn}\dot{s}) + 2kA\frac{\pi^2}{\lambda^2}\sin\frac{\pi}{\lambda}|s|\left(w - 2A\sin\frac{\pi}{\lambda}|s|\right)^{-}\frac{1+\tan^2(\alpha_C + \varphi\cdot\operatorname{sgn}\dot{s})}{1+\tan^2\alpha_C} \end{aligned} \tag{18}$$

Finally, the joint's element stiffness matrix in the global reference system is obtained as

$$\mathbf{K}_G = \mathbf{R}^T\cdot\mathbf{K}\cdot\mathbf{R} \tag{19}$$

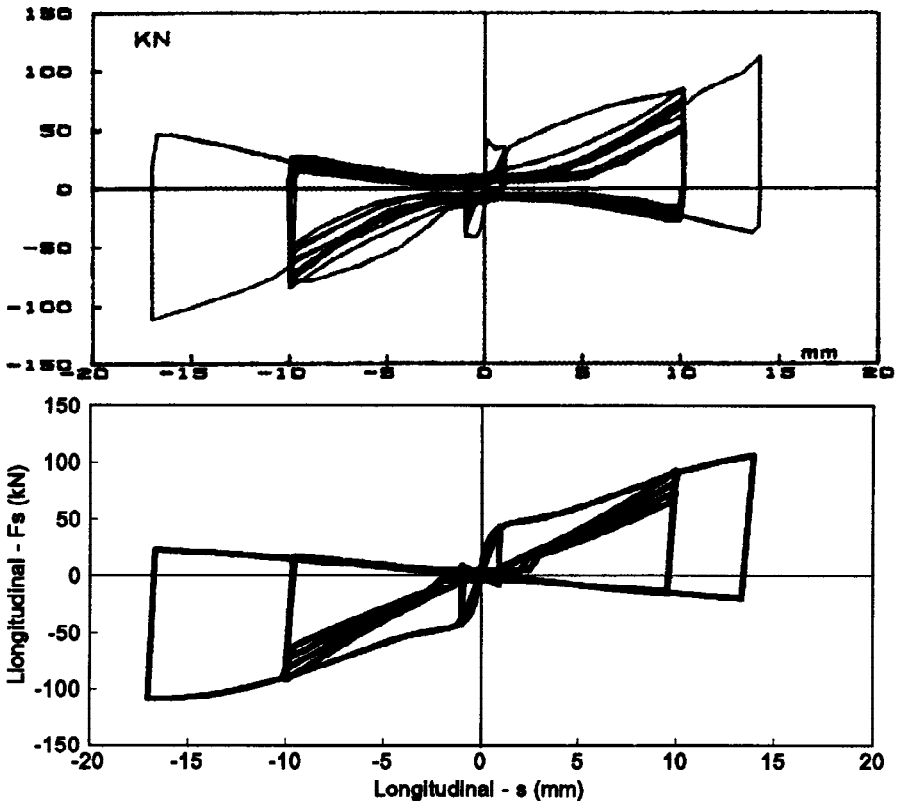

Fig. 7. Shear force vs. sliding for a cyclic test on a joint: experimental (above) and numerical (below) test.

CORRELATION STUDIES

Correlation studies with experimental tests have been performed with a preliminary model based on the governing equations developed above. As a starting point, the cyclic tests conducted on isolated specimens (Fig. 1) were reproduced, as shown in the example in Fig. 7. The governing equation adopted includes the profile damaged as from Fig. 3.
The numerical tests present satisfactory agreement with the experimental ones. In quantitative terms, the resisting force of the joint is correctly predicted, both for small and large amplitude cycles. The increase in resistance with the increase of displacement is also well reproduced. This is an extremely beneficial feature of the joint. Also after several cycles with constant amplitude, where a certain decrease in resistance is observed, due to profile scraping, when larger displacements are imposed, contact moves on points of the profiles which are still intact (not abraded), so that the resisting force can increase. Another important phenomenon, also related to the above mentioned mechanism, is the curvature inversion of the load branches following the first one. This is due to the hollows of the scraped profiles which present a reverse curvature with respect to the original sinusoid, as shown in Fig. 3.

CONCLUSIONS

The experimental research led to comprehensive and favorable results. It showed that the use is possible of untopped floors with grouted joints as diaphragms under severe seismic conditions. The behavior of the tested joint, with waved profile, demonstrated to meet all the requirements of resistance, "ductility", "strain-hardening" and little sensitivity to low-cycle fatigue. In seismic areas, untopped slabs are beneficial in that they reduce the response by saving mass.

From the analytical viewpoint, the developed model of the joint's behavior is reliable and accurate. Its incorporation into a finite element of the joint itself represents an essential component for the simulation of complete decks, which will allow to avoid more experimental tests, expensive and time-consuming, and to implement an easier and more comprehensive investigation campaign based on numerical testing, for assessing the effectiveness of in-plane behavior of precast floors of different shape, dimension and features.

REFERENCES

Menegotto M. and Morelli G. (1984). Shear tests on longitudinal joints of precast slabs, Proc. CTE Congress, Firenze (in Italian)

Menegotto M. (1988). Hollow-core floors tests for seismic action, Proc. FIP Symposium, Israel, Sept.

Menegotto M. and Monti G. (1988). Diaphragm behavior of precast floors subject to seismic action, Proc. CTE Conference, Venezia, Oct. (in Italian)

Menegotto M. (1994). Seismic diaphragm behavior of untopped hollow-core floors, Proc. FIP XII Congress, Washington D.C., U.S.A., May

Menegotto M. and Monti G. (1995). Modelization of waved joint for precast floor diaphragms, Proc. VII Conference on Earthquake Engineering in Italy, Siena, Sept. (in Italian)